Effects of Pulse Shape on rf SQUID Quantum Gates

Zhongyuan Zhou, Shih-I Chu, and Siyuan Han

***Abstract*—Effects of control-signal microwave pulse shapes on rf SQUID quantum gates are investigated. It is shown that the gate operations are mainly affected by microwave pulse area and are independent of pulse shape in the weak field limit.**

***Index Terms*—Pulse shaping methods, quantum computers, SQUID qubits.**

I. Introduction

RECENTLY, quantum computing has stimulated strong interests because of its potential for solving problems that are intractable for conventional computers. Among the many approaches, building quantum computers with the use of superconducting qubits is considered very promising because the intrinsically high degree of coherence of the Cooper pair condensate, the ability of engineering qubits with desirable properties, and the high potential for scaling up. Furthermore, superconducting qubits can be driven by pulsed microwaves to perform various 1-bit and 2-bit quantum gate operations required for processing quantum information. In this work we study the effects of pulse shape on the 1-bit rotation of SQUID qubits by evaluating intrinsic gate errors using rectangular-shaped pulses (ideal) and pulses with finite rise and fall times (realistic). We found that in the weak field limit there essentially is no difference between the rate of intrinsic gate errors (i.e., errors that exist without decoherence) for the ideal and realistic pulse shapes. Namely, the angle of 1-bit rotation depends only on the pulse area. However, at higher field intensity the gate error rate caused by pulses with finite rise and fall times become greater than that of the ideal pulses with the same pulse area. Our result shows that the increased error rate is due entirely to the effects of applying strong fields.

II. Theoretical Method

A. Theoretical Model of an rf SQUID

An rf SQUID qubit consists of a superconducting ring of inductance L closed with a Josephson tunnel junction. Applying the resistively-shunted junction (RSJ) model [1], the junction is characterized by its critical current I_c, shunt capacitance C and shunt resistance R. The Hamiltonian of the SQUID qubit is

$$H_0(x) = \frac{p_x^2}{(2m)} + U(x), \tag{1}$$

Manuscript received August 6, 2002. This work was supported in part by the NSF (grant no. EIA-0082499) and by AFOSR and ARDA (F49620-01-1-0439).

The authors are with the Department of Chemistry, University of Kansas, Lawrence, KS 66045 USA (e-mail: zyzhou@ku.edu; han@ku.edu; sichu@mail.ukans.edu).

Digital Object Identifier 10.1109/TASC.2003.814120

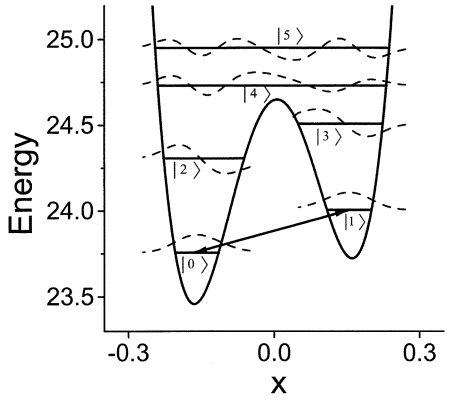

Fig. 1. Potential energy and the first six energy levels of a SQUID with $L = 100$ pH, $C = 40$ fF, and $I_c = 3.95\ \mu$A ($Z_0 = 50\ \Omega$, $\beta_L = 1.2$, and $\omega_{LC} = 5 \times 10^{11}$ rad/s). The flux bias $x_e = -0.501$.

where the potential energy is given by [2]

$$U(x) = \frac{1}{2}m\omega_{LC}^2(x - x_e)^2 - \frac{m\omega_{LC}^2}{4\pi^2}\beta_L \cos(2\pi x). \tag{2}$$

Here, $m = C\Phi_0^2$ is the mass of the fictitious "flux" particle, $x = \Phi/\Phi_0$ is the particle's position, Φ is the total magnetic flux enclosed in the SQUID loop, $\Phi_0 = h/2e$ is the flux quantum; $x_e = \Phi_e/\Phi_0$ is the normalized external magnetic flux applied to the SQUID; $p_x = -i\hbar\partial/\partial x$ is the momentum operator conjugate to x, $\omega_{LC} \equiv 1/\sqrt{LC}$ is the characteristic frequency of the SQUID, and $\beta_L = 2\pi L I_c/\Phi_0$. Equation (2) shows that the shape of the SQUID potential is determined uniquely by the dimensionless parameter β_L and the external flux x_e. In the presence of an external flux the SQUID generates a superconducting current circulating the loop to keep the total number of fluxoids q in the SQUID quantized. For $x_e = 1/2$, the potential has symmetric double wells. The left (right) well corresponds to the $q = 0$ $(q = 1)$ fluxoid state. Increasing (decreasing) x_e slightly from 1/2 tilts the potential to the right (left) that provides an easy way to control the potential and interwell level separations of the SQUID qubit (Fig. 1).

The eigenenergies E_n and eigenstates $|n>$ of a SQUID qubit can be obtained by numerically solving Schrödinger's equation with the anharmonic Hamiltonian $H_0(x)$. It has been shown that the eigenstates depend only on two independent SQUID parameters: the potential shape parameter β_L and the characteristic impedance $Z_0 \equiv \sqrt{L/C}$, while the eigenenergies are scaled to $\hbar\omega_{LC}$ [3]. The potential and the energy levels of a SQUID with $Z_0 = 50\Omega$ (i.e., $L = 100$ pH, and $C = 40$ fF), $\beta_L = 1.2$, and $\omega_{LC} = 5 \times 10^{11}$ rad/s are plotted in Fig. 1 for external flux $x_e = 0.501$.

B. Operation by Microwave Pulses

The conventional two-level SQUID qubit utilizes the lowest level in each of the double wells, denoted as $|0>$ and $|1>$ in Fig. 1, as the computational basis. Unitary transformations required to accomplish 1-bit rotations, such as the Hadamard and NOT gates, are implemented by controlling the pulse area of microwaves with frequency tuned to the level separation. The interaction between the SQUID and the microwave pulse, treated here as a linearly polarized electromagnetic field with its magnetic field component perpendicular to the plane of the SQUID loop, is

$$V(x,t) = m\omega_{LC}^2(x-x_e)\phi_\mu f(t)\sin(\omega_\mu t) + \frac{1}{2}m\omega_{LC}^2\phi_\mu^2 f^2(t)\sin^2(\omega_\mu t), \quad (3)$$

for $0 < t < \tau_\mu$ and zero otherwise. Here, ω_μ, ϕ_μ, τ_μ, and $f(t)$ are the frequency, amplitude (normalized to Φ_0), duration, and the shape factor of the microwave pulse. The total Hamiltonian of the system, $H(x,t) = H_0(x) + V(x,t)$, is now time-dependent. The time evolution of the system can be obtained by numerically integrating the corresponding time-dependent Schrödinger equation (TDSE)

$$i\hbar\frac{\partial\psi(x,t)}{\partial t} = [H_0(x) + V(x,t)]\psi(x,t). \quad (4)$$

C. Numerical Algorithms

To compute the evolution of the eigenstate populations of the SQUID qubit, the time-dependent wave function is expanded in the eigenstates $|n>$ of $H_0(x)$:

$$\psi(x,t) = \sum_{n=0}^{N} C_n(t)\,|n\rangle, \quad (5)$$

where, N is the number of $H_0(x)$ eigenstates included in the calculation. The time-dependent expansion coefficients $C_n(t)$

$$i\frac{\partial}{\partial\tau}C_n(\tau) = \sum_{n'=0}^{N} H_{nn'}^R C_{n'}(\tau), \quad (6)$$

are obtained by solving the time-dependent matrix equation, where $\tau \equiv \omega_{LC^t}$ is the reduced time. The matrix elements H_{nn}^R of the reduced Hamiltonian are given by

$$H_{nn}^R = \frac{[E_n\delta_{nn'} + \langle n|V(x,\tau)|n'\rangle]}{\hbar\omega_{LC}}. \quad (7)$$

In general, the C_n are complex which can be divided into real and imaginary parts, $C_n(\tau) = R_n(\tau) + iS_n(\tau)$. Substituting this into (6), a canonical equation is obtained for coefficient vectors $\mathbf{R} = \{R_n\}$ and $\mathbf{S} = \{S_n\}$, which can be expressed in matrix form as

$$\frac{d}{dt}\begin{bmatrix}\mathbf{R}\\ \mathbf{S}\end{bmatrix} = \begin{bmatrix}\mathbf{0} & \mathbf{H}\\ -\mathbf{H} & \mathbf{0}\end{bmatrix}\begin{bmatrix}\mathbf{R}\\ \mathbf{S}\end{bmatrix}, \quad (8)$$

where, $\mathbf{H} = \{H_{nn'}^R\}$ is the reduced Hamiltonian matrix. Time evolution of the expansion coefficients can be obtained by solving the canonical (8) using the symplectic scheme [2]. The method is efficient and capable of providing accurate information about the dynamics of the SQUID qubit. The propagator of the second order explicit symplectic scheme is given by

$$\begin{cases}\mathbf{U}^k = \mathbf{R}^k + \frac{\Delta\tau\mathbf{H}^{k+1/2}\mathbf{S}^k}{2}\\ \mathbf{S}^{k+1} = \mathbf{S}^k - \Delta\tau\mathbf{H}^{k+1/2}\mathbf{U}^k\\ \mathbf{R}^{k+1} = \mathbf{U}^k + \frac{\Delta\tau\mathbf{H}^{k+1/2}\mathbf{S}^{k+1}}{2}\end{cases}, \quad (9)$$

where, $\mathbf{R}^k = \mathbf{R}(\tau^k)$, $\mathbf{H}^{k+1/2} = \mathbf{H}(\tau^{k+1/2})$ and so on, and $\Delta\tau$ is the time-step.

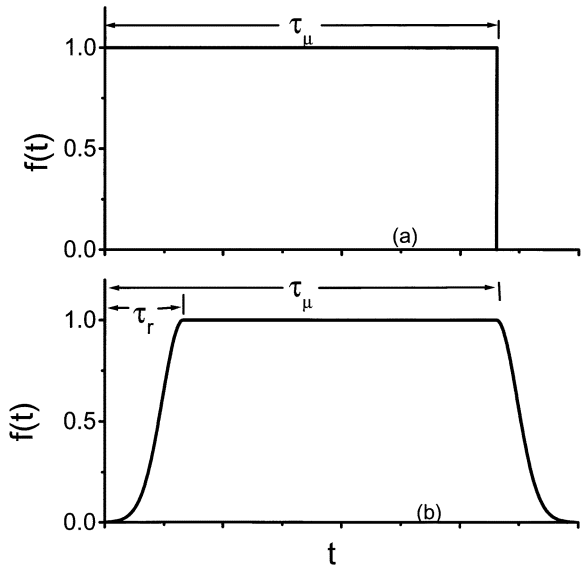

Fig. 2. Pulse shapes used in the computation. (a) Square pulse of duration τ_μ; (b) Gaussian-shaped pulse of duration τ_μ with equal rising (turn-on) and falling (turn-off) time τ_r.

III. Results and Conclusions

The gate operations of the SQUID qubits can be realized by applying microwave pulses. In ideal cases, the microwave pulses are square-shaped (with zero rise and fall times) and therefore the pulse durations required to accomplish desired quantum logic operations can be readily determined. However, real pulse shapes are always nonideal and have finite rise and fall times, which may have adverse effects on pulse-driven quantum gates. To study the effects of such pulse shapes on gate operations, we evaluate the gate speed and gate errors for different pulse shapes. For simplicity, the conventional 2-level SQUID qubits, *i.e.*, the states $|0>$ and $|1>$ in Fig. 1, are used as the computational basis. The conclusion here can be extended to optimized three-level qubits [2].

In this investigation, two types of pulse shape are used: (i) the square pulse (SP) with infinite sharp rising and falling edges, and (ii) pulse with Gaussian-shaped rising and falling edges (GP). The shape of GP is specified by the shape factor function

$$f(t) = \begin{cases}\exp\left[-6.91\left(\frac{t}{\tau_r}-1\right)^2\right] & (0 < t \le \tau_r)\\ 1 & (\tau_r > t \le \tau_\mu)\\ \exp\left[-6.91\left(\frac{(\tau_\mu - t)}{\tau_r}\right)^2\right] & (\tau_\mu < t \le \tau_\mu + \tau_r)\end{cases} \quad (10)$$

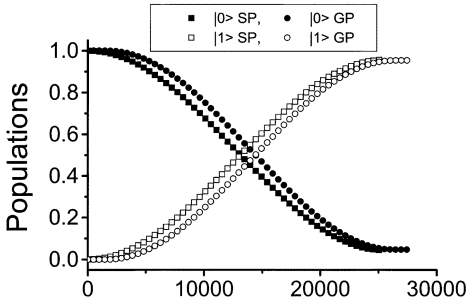

Fig. 3. Evolution of populations of the qubit states $|0>$ and $|1>$ for the SP and GP shapes. The solid (open) squares and circles are populations of the state $|0>(|1>)$ with the squares (circles) for the SP (GP) shape.

which are shown in Fig. 2. In our computations, the pulse duration is taken to be $\tau_\mu = 10^3$ T, where $T = 2\pi/\omega_\mu$ is the period of an "optical" cycle of the microwave, and the rise and fall times are set to $\tau_r = 10^2$ T. The same pulse area is used for both the SP and GP. The frequency of microwaves is tuned to the level separation.

In Fig. 3, the time evolution of the populations of qubit states $|0>$ and $|1>$ are shown for π pulses. It is interesting to notice that although the amplitude of GP is slightly larger than that of SP (see Fig. 4(b)) for the same pulse area, the gate speed of GP is slightly slower than that of SP because of the finite falling time of GP (Fig. 1(b)). However, the populations of the qubit states $|0>$ and $|1>$ at the end of the pulses are essentially the same for both pulse shapes. Therefore, in weak field regime nonideal pulse shape works as well as the ideal SP shape as long as its effect on pulse area is taken into account. However, this conclusion is not valid for strong fields as demonstrated by the results in Fig. 4.

In Fig. 4(a) the numerically calculated populations of the $|0>$ and $|1>$ states as a function of pulse area are shown for both SP and GP. In these calculations the pulse duration was kept constant and the pulse area was adjusted by varying microwave amplitude as shown in Fig. 4(b). The results presented in Fig. 4 clearly show that for small pulse areas, where the microwave fields are weak, the populations at the end of the pulses are in good agreement with each other for both pulse shapes and the intrinsic gate errors are negligible. However, for larger pulse areas intrinsic gate error becomes significant for both pulse shapes.

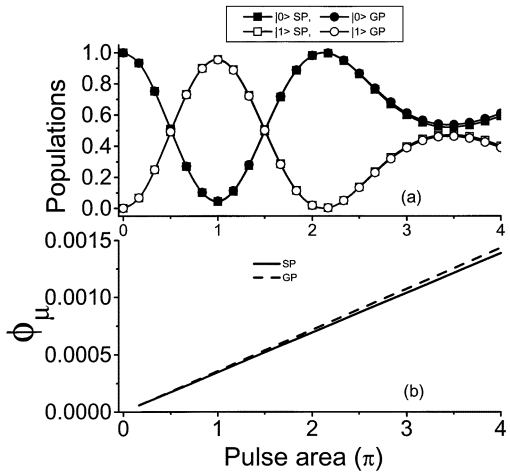

Fig. 4. (a) Populations of the qubit states $|0>$ and $|1>$ vs the pulse area. Solid (open) squares and circles are populations of the state $|0>$ ($|1>$) with the squares (circles) for the SP (GP). (b) Amplitude of the microwaves vs the pulse area. The solid (dashed) line is the amplitude of SP (GP).

Note that the slightly higher error rate of GP is due to the fact that for the same pulse area the field intensity of GP is higher than that of SP.

In summary, we investigated the effects of microwave pulse shapes on the quantum 1-bit gate operations of conventional 2-level SQUID qubits by comparing the populations of the qubit states at the end of microwave pulses for different pulse shapes with the same pulse area. It is found that the gate errors are essentially independent of the pulse shapes in the weak field limit. Our result also shows that when the weak field condition is not satisfied the larger gate error rate of GP can be accounted for entirely by the larger field amplitude required by GP.

REFERENCES

[1] D. E. McCumber, "Tunneling and weak-link superconductor phenomena ahaving potential device applications," *J. Appl. Phys.*, vol. 39, p. 2503, 1968.

[2] Z. Zhou, S. I. Chu, and S. Han, "Quantum computing with superconducting devices: A three-level SQUID qubit," *Phys. Rev. B*, vol. 66, p. 054 527, 2002.

[3] S. Han and R. Rouse, "SQUID qubits and quantum gates," in *Proc. of the NATO Advanced Research Workshop on Decoherence and its Implications Quantum Computation and Quantum Information Transfer*, Amsterdam, 2001, pp. 317–328.